PAPER

Synchronized switch piezoelectric energy harvesting using rotating magnetic ball and reed switches

IOP Publishing Smart Materials and Structures
Smart Mater. Struct. **30** (2021) 105023 (9pp) https://doi.org/10.1088/1361-665X/ac1f62

Synchronized switch piezoelectric energy harvesting using rotating magnetic ball and reed switches

Yongji Gao[1,2,3], Guobiao Hu[1,*], Bao Zhao[1], Kunyong Lv[1] and Junrui Liang[1,*]

[1] School of Information Science and Technology, ShanghaiTech University, 393 Middle Huaxia Road, Shanghai 201210, People's Republic of China
[2] Shanghai Institute of Microsystem and Information Technology, Chinese Academy of Sciences, Shanghai 200050, People's Republic of China
[3] University of Chinese Academy of Sciences, Beijing 100049, People's Republic of China

E-mail: guobiao_hu@outlook.com and liangjr@shanghaitech.edu.cn

Received 28 December 2020, revised 26 July 2021
Accepted for publication 19 August 2021
Published 2 September 2021

Abstract

Synchronized switch harvesting on inductor (SSHI) interface circuit has been developed to boost the harvesting capability of piezoelectric energy harvesters (PEHs). Although some electronic self-powered peak-detector and switching circuits have been proposed to support the practical realization of SSHI, the energy dissipation and voltage drops in transistors and diodes of the self-powered circuits might significantly deteriorate the actual energy harvesting performance. Some mechatronic designs were proposed as well. However, most of their switches are activated by touch impacts, which might introduce undesired high-order vibrations to the main structure. In this paper, rather than using the impact-engaged strategy discussed in the literature, a new mechanism using a magnetic ball for vibration synchronization and reed switches for switching operation is proposed. A PEH shunted to an SSHI interface circuit using the proposed mechatronic approach has been prototyped. Since the peak-detection and switching operations are completed by a mechanical mechanism, less passive electrical components, which consume extra energy, are required in our proposed design. Therefore, the overall energy harvesting performance is improved. Numerical simulations and experimental tests have validated the feasibility of the proposed design. The experimental results have shown that the power output produced by the proposed mechatronic self-powered SSHI design can be increased by 80% and 25%, as compared with the cases using a benchmark standard energy harvesting bridge rectifier and an electronic self-powered SSHI solutions, respectively. Moreover, owing to the new mechatronic design, the auxiliary mechanical components are embedded in the tip block of the cantilevered PEH, rendering the whole system to be a compact design.

Keywords: piezoelectric energy harvesting, reed switch, synchronized switch, interface circuit

(Some figures may appear in colour only in the online journal)

1. Introduction

Over the past two decades, harvesting vibration energy from the ambient environment to power distributed wireless sensor networks has attracted extensive research interest [1–6]. Among various sustainable energy solutions, piezoelectric energy harvesting (PEH) has been extensively explored due to its advantages of high-power density and ease of implementation. The energy harvesting circuit used can play an important role in improving the performance of an energy harvester. To boost the energy conversion efficiency, advanced interface

* Authors to whom any correspondence should be addressed.

circuits, such as synchronized switch harvesting on inductor (SSHI) [7, 8], synchronous electric charge extraction [9–11], and their hybrid combinations [12] were proposed. It has been experimentally proven that, compared with conventional standard circuits, using an SSHI circuit can improve the power output of a piezoelectric energy harvester by severalfold [7].

In an SSHI interface circuit, a synchronized switching operation is carried out when the piezoelectric voltage reaches its maximum or minimum. The switching operation results in the connection of the piezoelectric transducer to an external inductor, forming a resistance-inductance-capacitance (RLC) resonant branch. Given such a newly connected circuit path, the piezoelectric voltage immediately encounters a transient under-damped oscillation. If we disconnect the switch after about half of the RLC cycle, the piezoelectric voltage will stay at the largest overshoot value. With these synchronized switch actions, the piezoelectric voltage and equivalent current can be guaranteed to have the same sign along each vibration cycle. Therefore, the extracted power from the piezoelectric transducer is always positive, i.e. doing positive work to the harvesting circuit. The power factor has been improved and more close to the unity [7].

From the working principle of SSHI, it can be known that, how to detect the voltage peaks and carry out the switching actions are the two key issues for realizing the voltage inversions in time. In the early study of SSHI, based on the fact that the piezoelectric voltage is basically proportional to the displacement of the piezoelectric structure, a displacement sensor was used for peak detection [7]. Moreover, a controller was utilized to execute the switching tasks. These auxiliary devices inevitably need to consume energy. It is very likely to require external power supplies to run these devices. From the energy point of view, by taking account of the consumed energy by the auxiliary devices, the real effectiveness of SSHI interface circuit is actually questionable. Such a doubt existed until the introduction of the electronic self-powered version of SSHI (ESP-SSHI) [13–15]. The ESP-SSHI circuits are built with two envelop detectors and some switching transistors, whose switching moments are specifically designed at voltage peaks. The advantage of ESP-SSHI interface circuits and its practicability were extensively recognized by the research community. The ESP-SSHI scarifies some performance for carrying out the self-powered function. For example, the voltage drops in practical diodes and transistors cause some energy dissipation and also increase the delay of switch instants [16]. These factors will decrease the inversion factor, which results in a reduction in piezoelectric voltage amplitude and therefore counteracts the harvesting capability improvement [14, 17]. New circuit designs kept emerging for restoring the improvement effect of the original SSHI against the energy loss in self-powered electronic switches [18, 19].

To automatically carry out the SSHI functions, some mechatronic solutions using mechanical switches have also been proposed in recent years. Compared with the active switching components, i.e. transistors, used in the ESP-SSHI solutions, mechanical switches have no threshold voltage nor voltage drop. Hence, the energy dissipation in the switching components can be eliminated; the switching delay can be also reduced with a proper mechatronic dynamic design. According to the literature, most existing mechanical switches used in mechatronic self-powered SSHI (MSP-SSHI) are realized based on an impact-engaged strategy, such as the contacting stopper designs [20–23]. The switch electrodes, which forms the temporary RLC branch in SSHI, are designed at the contacting points of the oscillator and stopper. Once the oscillator hits the stopper around the maximum displacement points, the electrodes are forced into contact and the switching operation is, thereby, carried out. However, for most of the stopper designs using the impact-engaged strategy, the vibration amplitude can be neither too large nor too small [24]. In case of a small amplitude vibration, the oscillator can not touch the stopper, so the switch can not be turned on. In case of a large amplitude vibration, strong impacts between the oscillator and the stoppers may easily occur and result in structural damage. To address the above issues, Liu *et al* [24] introduced a two-degree-of-freedom (2DOF) design by modifying the hard stoppers in the main structure into a small peak-displacement switch as an auxiliary structure. Liu *et al* [25] proposed to use soft memory form, rather than stiff materials, to constitute the mechanical stopper. An alternative strategy to realize mechanical switch is by using the reed switches [17]. Reed switches are controlled by magnetic fields. By placing two reed switches near the maximum displacement positions of the oscillator and attaching a magnet at the free end of the oscillator, the non-contacting switch actions can be achieved during vibration. Compared with the impact-engaged strategy, by using the reed switches, on one hand, the structural collisions are evaded. On the other hand, provided that a reed switch has a larger effective zone near the magnetic field, the switching actions have a larger possibility to be activated, compared with the point-contacting moving oscillator and stopper.

No matter for the hard stopper designs [20, 21, 23] or the reed switch designs [17], the switching positions are not exactly the maximum displacement positions. The soft stopper design [25] performs better even with slow magnitude variation. For all these designs, additional frames are needed besides the main structure for installing those contacting stoppers or reed switches. In this sense, the 2DOF MSP-SSHI solution is more likely to be made into compact designs.

In this article, we combine the benefits of the 2DOF design (compact and can freely move) and the reed switch design (non-impact and large effective zone) toward the proposal of a new MSP-SSHI design. Compared with the original 2DOF design [24], the impacting vibration sensing switch is replaced with a new rotating non-impact assembly, which is composed of a circular track, a magnetic ball, and a pair of reed switches. A reed switch consists of a pair of ferromagnetic flexible metal contacts. Once a magnetic field is applied, the two contacts will close, and the switch will be turned on. Because the magnetic attraction force between the ball and reed switch is much larger than the rolling friction force between the ball and track, once the ball and reed switch get closer, either the south or north pole of the magnetic ball will be automatically attracted to face the reed switch, such that to properly turn it on. The circular track is engineered to allow the magnetic ball to eventually achieve a periodic motion when the whole main

structure enters steady-state vibration. Both the peak detection and switching operation are completed along with the relative rotation of the magnetic ball. Therefore, the collision behavior does not exist anymore in this proposed design.

2. Design

Figure 1 shows the prototype of the PEH using the proposed MSP-SSHI interface design. The proposed PEH consists of a piezoelectric cantilever beam and a tip block. Inside the tip block, a closed track is engineered to hold a magnetic ball and let it move in a circular trajectory. A pair of reed switches are respectively installed on the top and bottom of the tip block, outside but close to the closed track. Once the whole system is excited by an external base excitation, the magnetic ball inside the tip block is driven to smoothly roll along the circular trajectory confined by the closed track. It is expected that the symmetric design of the closed track could enable the magnetic ball to finally move in a periodic circular motion. At steady state, when the tip block reaches the maximum points, the magnetic ball should concurrently arrive at the polar positions, i.e. top or bottom of the circular track. Hence, the proposed mechanical assembly hopefully can carry out self-powered peak detection. The two reeds of a reed switch are two ferromagnetic bodies of which can be magnetized into two polar under a magnetic field. When the magnetic field is strong enough to overcome the restored elastic force between the two reeds, the reed switch can be conducted. Therefore, the conduction of reed switch is more related with the magnetic field strength rather than the polarization of the magnetic ball.

When the magnetic ball rapidly passes by either of the polar positions, due to the magnetic force, the top or bottom reed switch would be consequently triggered on for a short instant. The switching operation could thus be passively completed. By integrating the reed switches with the SSHI interface circuit and the piezoelectric transducer, the synchronized switch harvesting can, therefore, be realized. As compared with the previous designs in the literature [24, 25], this new design has no mechanical stopper. The magnetic ball and the reed switches are installed inside the tip block, making the whole system to be a more compact design. Moreover, since the peak detection relies on the engineered circular rolling motion and due to the use of the non-contacting reed switches, hard collisions can be avoided.

Figure 2 describes the whole working process step by step to help understand the working principle of the proposed mechatronic design. In figure 2(a), the deformation of the piezoelectric cantilever beam reaches a maximum. At this moment, the peak voltage is attained, and the magnetic ball should be designed to synchronously pass by the top of the circular track in the tip block, where a reed switch is installed. As the magnetic ball approaches the upper reed switch, the magnetic effect becomes sufficiently strong to turn on the reed switch. Consequently, the circuit path that consists of diode D_5 and inductor L_i is conducted. The conduction of this inductive path results in the discharge of the piezoelectric

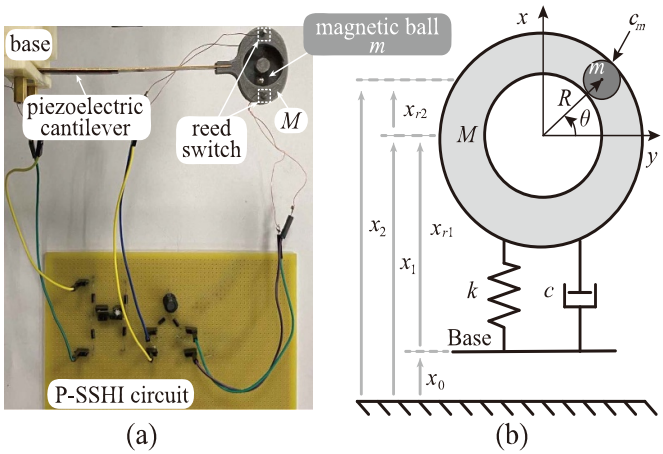

Figure 1. (a) A PEH shunted to the MSP-SSHI design using rotating magnetic ball and reed switches. (b) The abstracted lumped parameter model of the mechanical structure.

capacitance C_p through an under-damped transient electrical response. The charge in C_p flow through the inductor L_i. Since a small inductor is usually used, the RLC cycle is relatively small, compared with the mechanical cycle. The voltage inversion (overshoot) can be regarded as being completed in an instant. After the magnetic ball rolls away, the reed switch is turned off. The turn-on time of the reed switch in this case is usually longer than the required transient (a half of the L_i-C_p cycle) for inverting v_p. The diode D_5 prevents the reverse current through the C_p and L_i branch. Therefore, the piezoelectric voltage v_p stops at the maximum overshoot after such a switch operation.

After the maximum deflecting position, the system enters the state as shown in figure 2(b). The piezoelectric cantilever beam pass through its equilibrium position downward at its maximum speed. The relative velocity of the tip block reaches the maximum. Its relative acceleration becomes zero. The magnetic ball should approximately arrive at the left or right end of the track. Since the ball speed is tangent to the track outline, there is no force applied on the ball in the x direction. Since the magnetic ball is away from both reed switches, at this moment, all reed switches are turned off. The current might flow though the highlighted circuit path to charge the capacitor C_r, if the maximum piezoelectric voltage v_p is larger than the rectified direct current (DC) voltage v_r across C_r. The diode D_1 and D_3 on this path play the role in regulating the current.

Figures 2(a) and (b) illustrate the process in a half vibration cycle. Figures 2(c) and (d) illustrate the process in the other half cycle. Under steady-state vibration, the movement in the latter half cycle is symmetric to that in the former half cycle. Therefore, the operation steps illustrated in figures 2(c) and (d) are not repeated here. Generally speaking, owing to the synchronization design between the motions of the tip block and the magnetic ball, peak detection is realized through this mechanical design. In this design, no transistors and diodes are needed to build electronic peak detectors and comparators [16, 17]. As there are less passive electrical components being

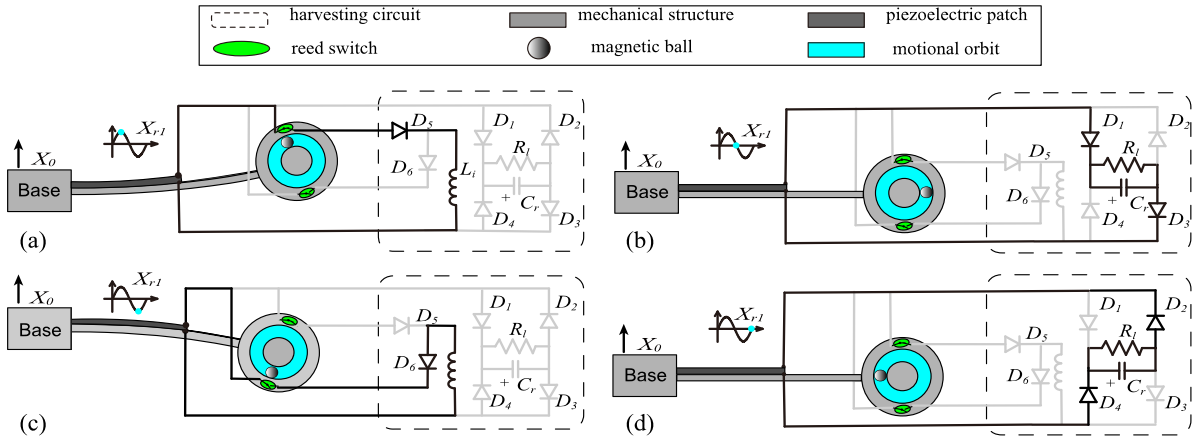

Figure 2. Working cycle of the proposed design from (a) to (d). (a) The instant when the tip block reaches the maximum displacement in the positive direction. The magnetic ball synchronously arrives at the top of the circular track. (b) The instant when the tip block returns to the equilibrium position. The magnetic ball arrives at the right-hand-side of the track. The accelerations of both the tip block and magnetic ball synchronously become zero. (c) The instant when the tip block reaches the maximum displacement in the negative direction. The magnetic ball synchronously arrives at the bottom of the circular track. (d) The instant when the tip block returns to the equilibrium position. The magnetic ball arrives at the left-hand-side of the track. The accelerations of both tip block and magnetic ball synchronously become zero.

used in this proposed MSP-SSHI solution, the energy dissipation in the power conditioning circuit is reduced. The energy harvesting efficiency is improved.

3. Modeling

A dynamic model is built to better understand and evaluate the dynamics of this system. As we know, a cantilever beam can be abstracted as a 1DOF system around its fundamental resonance. The rigorous mathematical proof of the equivalent between a piezoelectric cantilever beam and a 1DOF model can be referred to [26]. By adopting the 1DOF model of the piezoelectric cantilever beam, the mechanical structure of the proposed energy harvesting system is simplified as shown in figure 1(b). The closed track is implemented in the horizontal plane, which is perpendicular to the direction of gravity. Thus, the circular rolling motion of the magnetic ball is not affected by the gravity. M denotes the equivalent mass of the cantilever beam together with the tip block. m is the mass of the magnetic ball. k is the stiffness of the cantilever beam. c is the damping coefficient of the cantilever beam. c_m is the friction coefficient between the magnetic ball and the circular track, which is very small and usually neglected. R is the radius of the circular track. θ is the angle describing the position of the magnetic ball. The excitation is assumed to be only in the x direction. Through coordinate transformation, the position of the magnetic ball can be described in Cartesian notation as $x_2 = x_1 + R\sin\theta$ and $y_2 = -R\cos\theta$. x_1 donates the absolute displacement of the tip block in the x direction. x_2 and y_2 denote the displacements of the magnetic ball in the x and y directions, respectively. Therefore, the kinetic energy T, potential energy V and Lagrange function of the whole system can be expressed as follows

$$T = \frac{1}{2}M\dot{x}_1^2 + \frac{1}{2}m\left(\dot{x}_2^2 + \dot{y}_2^2\right) + \frac{1}{2}J_m\left(\frac{\dot{\theta}R}{r}\right)^2; \tag{1}$$

$$V = \frac{1}{2}kx_{r1}^2; \tag{2}$$

$$L = T - V = \frac{1}{2}(M+m)\left(\dot{x}_{r1} + \dot{x}_0\right)^2 + \left(\frac{1}{2} + \frac{1}{5}\right)mR^2\dot{\theta}^2 + mR\dot{x}\dot{\theta}\cos\theta - \frac{1}{2}kx_{r1}^2. \tag{3}$$

In equations (1)–(3), x_0 is the base displacement; x_{r1} is relative displacement of the tip block to the base; and x_{r2} is relative displacement of the magnetic ball to the tip block. $J_m = 2mr^2/5$ is the rotational inertia of the magnetic ball, r is the radius of the magnetic ball. Using the Lagrange's approach, the governing equations of the system can be written as follows

$$\begin{cases} (M+m)\ddot{x}_{r1} + mR\ddot{\theta}\cos\theta - mR\dot{\theta}^2\sin\theta \\ \qquad\qquad + kx_{r1} + c\dot{x}_{r1} = -(M+m)\ddot{x}_0; \\ \dfrac{7}{5}mR^2\ddot{\theta} + c_m\dot{\theta} + mR\ddot{x}_{r1}\cos\theta = -mR\ddot{x}_0\cos\theta. \end{cases} \tag{4}$$

From the governing equations, it should be noted that the circular motion of the magnetic ball, i.e. θ, is coupled with the displacement of the tip block, i.e. x_{r1}. Given an external base excitation, the circular motion of the magnetic ball will be stimulated, since x_{r1} varies with time under such an excitation. Besides, from equation (4), it is known that the maximum inertia of moment of the ball is proportional to the external excitation amplitude. If the radius of the circular track is increased, the rotational acceleration of the ball will decrease. Consequently, the ball may not have sufficient energy and will sway at the bottom of the circular track around the static equilibrium position. To enable the magnetic ball to easily conduct a full circular motion, the track radius should not be designed too large.

Table 1. Parameters of the experimental setup.

Parameters	Value	Parameters	Value
k (N m^{-1})	42.35	c (Ns m^{-1})	0.016
M (g)	5.1	m (g)	0.5
f_0 (Hz)	14.5	γ	-0.5
C_p (nF)	30.8	C_r (μF)	4.7
L_i (mH)	10	r_{L_i} (Ω)	13.5
Magnetic ball remanence (T)	1.4	Reed switch (mm)	$\Phi 3 \times 20$

γ is the voltage inversion factor [26], which is measured in experiment.

4. Simulation and experiment

Numerical simulation and experiment are carried out to investigate the actual dynamic behavior of the proposed design. Figure 1(a) shows the physical prototype of the proposed PEH shunted to an SSHI interface circuit driven by rotating magnetic ball and reed switches. The piezoelectric cantilever beam consists of a piezoelectric bimorph (35 mm $\times$ 7 mm $\times$ 0.75 mm) and a copper substrate (100 mm $\times$ 10 mm $\times$ 0.4 mm). The radius of the circular track and the magnetic ball are 10 and 2.5 mm, respectively. The value of the radius of the circular track is determined by the numerical simulation based on equation (4). When the orbit radius is too large, it is difficult to complete a full circular motion. If the radius is too small, the magnetic ball will simultaneously affect the two reed switches and always conduct reed switches. The equivalent parameters of the 1DOF model of the cantilever beam based PEH and the parameters of the electrical components are listed in table 1. According to a preliminary experimental test, the natural frequency of the piezoelectric cantilever beam with the tip block but not the magnetic ball is identified to be 14.5 Hz.

Equation (4) is numerically solved using the Runge-Kutta method. The experimentally identified parameters of the prototyped system, which are listed in table 1, are adopted in numerical simulation. The excitation frequency and the acceleration magnitude are varied within a certain range to explore the feasibility of the expected working mechanism of the proposed system. Figure 3 presents the obtained numerical results. In figure 3(a), the x-axis and y-axis are frequency and acceleration magnitude, respectively. The circular symbols filled area denotes the feasible zone. In the feasible zone, synchronization between the motions of the oscillator and the magnetic ball can be achieved. It can be seen that when the acceleration level is sufficiently large and the excitation frequency is neither too small or too large, this design is feasible to carry out SSHI functions within the frequency range from 9 to 14 Hz, which is around the resonant frequency of the 1DOF PEH. There are two infeasible zones, in which the expected synchronization can not be achieved. One corresponds to the quiet cases (no switching action), which are filled by the triangle markers. The other infeasible zone corresponds to the irregularly moving cases, which are filled by the square markers. The possible explanation might be as follows. If either the acceleration level or excitation frequency is small, the magnetic ball is trapped by the magnetic force around either reed switch. Therefore, it is unable to complete the periodically rotating motion in the closed track. On the other hand, when the excitation frequency is larger beyond the resonant frequency, the expected synchronization is violated due to the irregular motion of the magnetic ball, because the magnetic ball cannot effectively follow the quickly vibrating frame. Therefore, in general, only under a proper acceleration level and around the resonant frequency, the synchronization phenomenon can successfully take place and the proposed system can operate as expected.

To give more insights into the dynamic responses in the feasible and infeasible zones, figures 3(b)–(d) show the phase portraits of the system when it works in different zones. The horizontal axis represents the normalized relative displacement of beam tip, i.e. $\tilde{x}_{r1}$. The vertical axis is $\sin\theta$. When $\sin\theta = \pm 1$, it indicates that the magnetic ball reaches the top or bottom of the circular track, respectively. Figure 3(b) shows the result when the excitation frequency is larger beyond the resonant frequency. The phase portrait in this case indicates a chaotic motion of the magnetic ball. Figure 3(c) shows the result when the acceleration magnitude is small or the frequency is smaller beyond the resonant frequency. It can be found that during the vibration of the PEH, $\sin\theta$ constantly equals to one. It indicates that the magnetic ball always stays at the top or bottom of the track; therefore, it fails to carry out a circular motion. Figure 3(d) shows the phase portrait of a successful case. It can be observed that the phase portrait follows a oblique curve that links the two extreme points, i.e. $(-1,-1)$ and $(1,1)$. According to the successful phase portraits for properly carrying out SSHI, it can be concluded that when $\tilde{x}_{r1}$ reaches its maximum (minimum), $\sin\theta$ must synchronously reach around its maximum (minimum).

The manufactured prototype is also tested in the same frequency range from 8 to 15 Hz and acceleration levels from 2 to 10 m s^{-2}. The corresponding experimental results are illustrated in figure 4. The feasible/infeasible zones in experiment are labeled with the same markers as those in figure 3. The experimental result basically agrees with the numerical prediction. Figures 4(b)–(d) shows the representative cases of the piezoelectric voltage v_p in three different working zones. When operates in the square zone (high-frequency zone beyond the resonance), the PEH undergoes chaotic motions. The corresponding v_p waveform is shown in figure 4(b) in irregular shape. Such a chaotic motion is caused by the irregular movement and collisions of the magnetic ball with the circular track. Switching actions are carried out from time to time, as we can observed from the figure. When the acceleration is small or frequency is much lower the the resonant one, the PEH operates in the triangular zone. The corresponding v_p waveform is shown in figure 4(c). The voltage magnitude is small. In the experiment, we observe that the magnetic ball always stays at the bottom of the circular track, which is the same as the numerical method predicted. In the zone labeled by circles, the system can successfully carry out SSHI operation. The corresponding v_p waveform is shown in figure 4(d). As we can observe from the figure, the voltage v_p can be inverted when reaching its maximums or minimums. There is slight switch phase lead within this feasible range when the frequency varies, the reason is that the reed switch needs to be

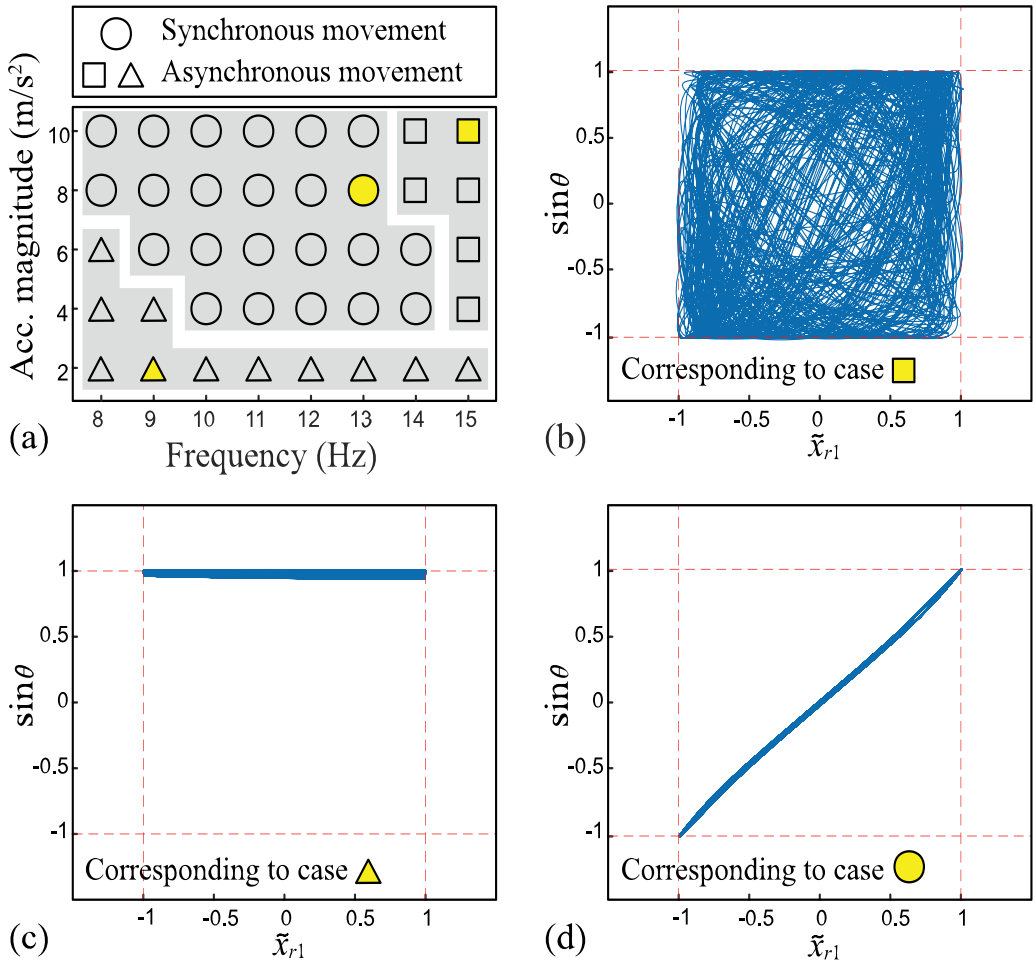

Figure 3. (a) The feasible/infeasible working zones obtained from simulation. (b) Phase portrait in an infeasible case under high-frequency excitation (square). (c) Phase portrait in an infeasible case under small-acceleration excitation (triangle). (d) Phase portrait in a feasible case (circle).

installed within the magnetic field of the magnetic ball in the experiment. Some trial-and-error tuning is needed to carefully choose the magnetic ball with an acceptable magnetic field strength, such that the switching action can be carried out on time once the voltage peaks are attained.

A comparative study is done to validate the advantage of this proposed MSP-SSHI design over the benchmark standard energy harvesting (SEH) circuit, i.e. a bridge rectifier. Under the excitation frequency of 13 Hz, the vibration acceleration is varied from 4 to 10 m s^{-2} and the load resistance is varied from 300 to 6000 kΩ. Figure 5 presents the comparison results in this experiment, in terms of output DC power. Both the MSP-SSHI design and SEH circuit give the maximum harvested power when the load resistance is round 800 kΩ. As expected, the MSP-SSHI design always produce larger power output than the SEH circuit. In all cases of our experimental study, the harvested power from MSP-SSHI is larger than that from the SEH circuit by at least 75%. For instance, the maximum harvested power from SEH is about 0.25 mW under the acceleration of 10 m s^{-2}. Under the same excitation condition, the maximum harvested power from MSP-SSHI is about 0.45 mW, which gives an 80% increase as compared with SEH.

In the next experiment, the acceleration is controlled constantly at 10 m s^{-2}, while the excitation frequency is varied from 12 to 15 Hz. The comparative results between MSP-SSHI and SEH are presented in figure 6. It can be seen that the MSP-SSHI design can always harvest more output than the SEH circuit within the frequency range we investigated. For example, when the excitation frequency is 14 Hz, the maximum power harvested by the MSP-SSHI and SEH solutions are 0.60 and 0.41 mW, respectively. Moreover, it is noted that, among those frequencies we investigated, the system generates the maximum power at the frequency of 14 Hz. However, 14.5 Hz is the resonant frequency of the PEH without the magnetic ball. The presence of the magnetic ball slightly alters the dynamic behavior of the whole system. Hence, the resonant behavior of the coupled system might be changed a little bit. Since the mass of the magnetic ball is much lower than the outer frame, its dynamic effect is negligible in this proof-of-concept stage. The dynamic interaction during the switching instants will be discussed in the future, if it has a significant influence to the operation, say when the ball weight is comparable to that of the frame mass.

Finally, a comparison between the proposed MSP-SSHI design and the ESP-SSHI circuit, which was proposed in

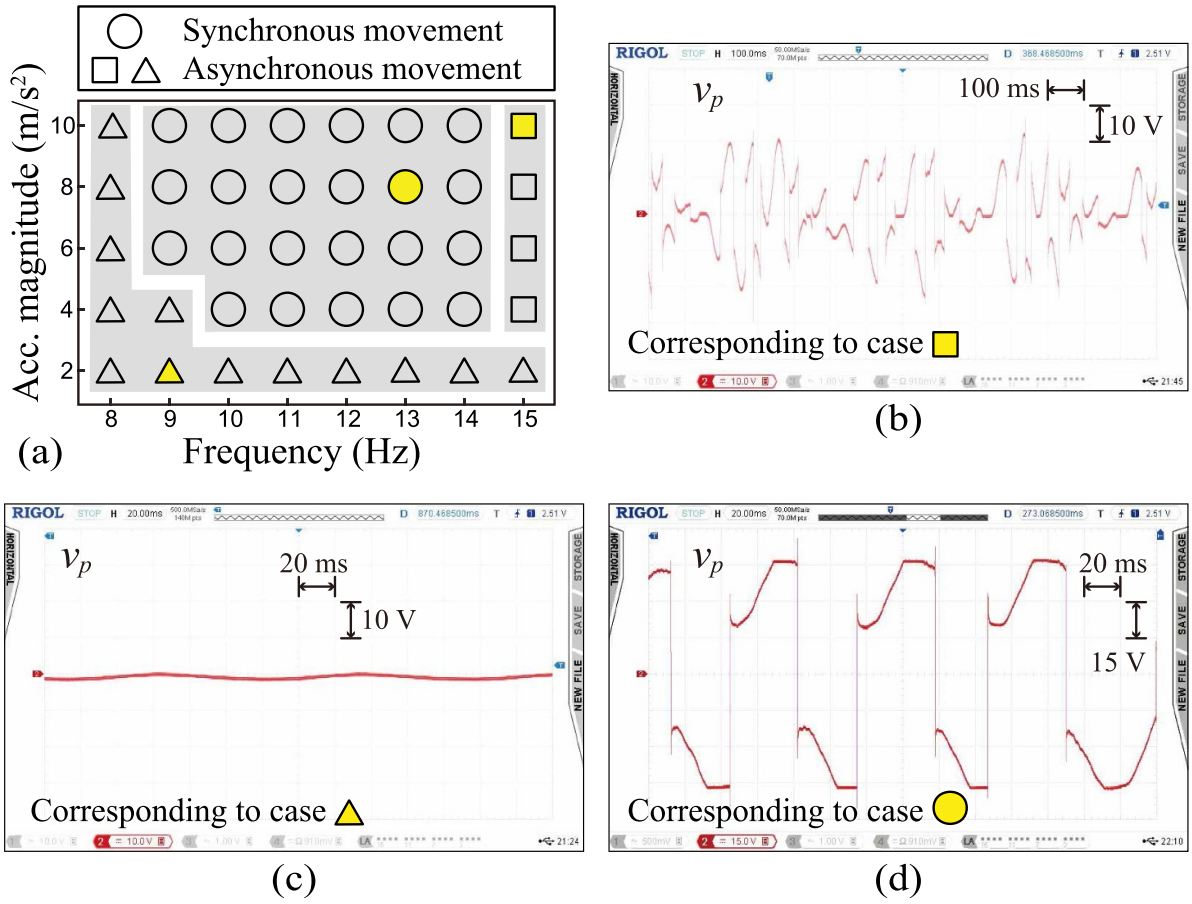

Figure 4. (a) The feasible/infeasible working zones observed from simulation. (b) v_p waveform in an infeasible case under high-frequency excitation (square). (c) v_p waveform in an infeasible case under small-acceleration excitation (triangle). (d) v_p waveform in a feasible case (circle).

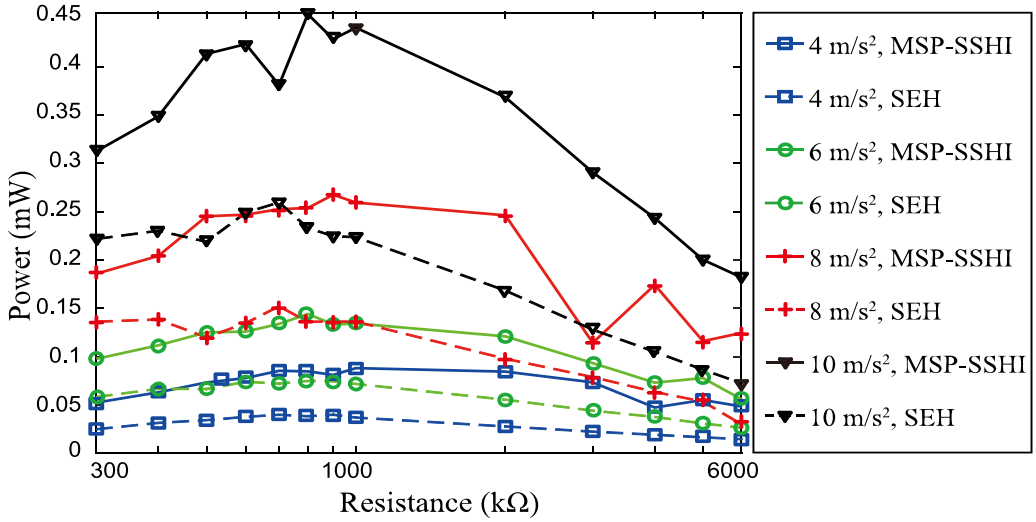

Figure 5. Harvested power comparison in experiment under different acceleration levels ($f = 13$ Hz).

[14], is also studied. Under the same excitation frequency 13 Hz, the harvested power under different acceleration levels is investigated and shown in figure 7(a). For fair comparison, the maximum harvested power under the optimal load resistance is considered among different frequency and acceleration conditions. By contrast, under the constant acceleration level of 8 m s^{-2}, figure 7(b) shows the harvested power results under different excitation frequencies. It is noted that, under the same operation condition, the proposed MSP-SSHI design can always harvest more power than the ESP-SSHI circuit. As revealed in figure 7(a), at the frequency of 13 Hz, the power output from the proposed MSP-SSHI design is larger than that from ESP-SSHI by at least 25%. The reason behind this phenomenon has already been explained in section 1.

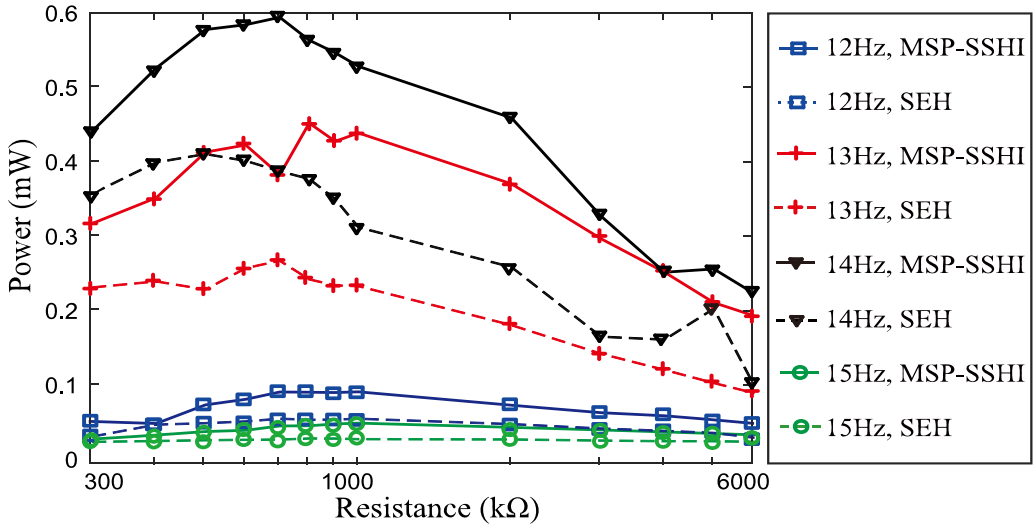

Figure 6. Harvested power comparison in experiment under different excitation frequencies (Acc = 10 m s^{-2}).

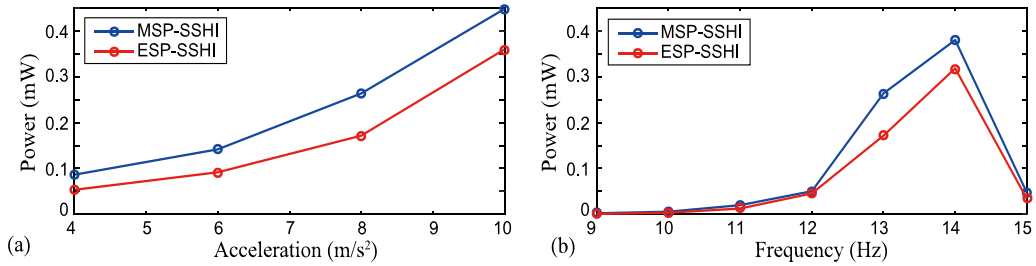

Figure 7. Comparison between experimentally obtained maximum harvested outputs from the proposed MSP-SSHI design and the ESP-SSHI circuit. (a) Under different accelerations levels and constant frequency 13 Hz. (b) Under different excitation frequencies and constant acceleration magnitude 8 m s^{-2}.

As less passive electrical elements are used in our proposed mechatronic self-powered design, more energy dissipation is reduced. The energy harvesting efficiency of the proposed MSP-SSHI circuit is thus improved. However, when the excitation frequency moves further away from the resonant frequency, for example at the frequency of 10 Hz as shown in figure 7(b), no obvious advantage is observed by using the proposed MSP-SSHI. Because, under excitation frequency far away from the resonant frequency, the vibration magnitude is small; the synchronized switch action cannot effectively improve the harvested power. In general, from the comparison shown in figure 7, the proposed MSP-SSHI design exhibits better performance than the ESP-SSHI circuit as we expected.

5. Conclusion

This article has presented a novel mechatronic approach to realize a compact and efficient synchronized switch PEH solution. A sophisticated structure, which contains a circular track, a rotating magnetic ball, and two reed switches, has been engineered to achieve this purpose. Different from those previous designs based on impact-engaged strategy, the circular motion of a magnetic ball does not cause any hard collision, which might affect the system dynamics. The motion synchronization between the piezoelectric structure and the magnetic ball at its free end has been employed for realizing peak detection. The switching actions are completed by using reed switches, which are installed at proper positions of the circular track.

The working principle of the proposed system has been explained in detail. To better analyze the system dynamics, a theoretical model has been developed based on the Lagrange's principle. Numerical simulations and experimental tests have been conducted with a prototyped system for proof-of-concept. The experimental results have shown that the proposed MSP-SSHI solution outperforms the benchmark SEH interface circuit (bridge rectifier without active switch) with a 80% power increase. Moreover, comparative results have also shown that, the proposed design can harvest 25% more power than the previously proposed ESP-SSHI circuit. In conclusion, the feasibility and benefit of the proposed design has been demonstrated and validated.

Data availability statement

All data that support the findings of this study are included within the article (and any supplementary files).

Acknowledgment

This work was supported by the grants from Natural Science Foundation of Shanghai (21ZR1442300), Shanghai Key Laboratory of Mechanics in Energy Engineering (ORF202001), and ShanghaiTech University (F-0203-13-003).

ORCID iD

Junrui Liang https://orcid.org/0000-0003-2685-5587

References

[1] Anton S R and Sodano H A 2007 *Smart Mater. Struct.* **16** R1
[2] Liang J and Liao W 2009 *J. Intell. Mater. Syst. Struct.* **20** 515–27
[3] Liang J and Liao W H 2010 *Smart Mater. Struct.* **20** 015005
[4] Harne R L and Wang K 2013 *Smart Mater. Struct.* **22** 023001
[5] Yang Z, Zhou S, Zu J and Inman D 2018 *Joule* **2** 642–97
[6] Li Z, Liu Y, Yin P, Peng Y, Luo J, Xie S and Pu H 2021 *Int. J. Mech. Sci.* **198** 106363
[7] Guyomar D, Badel A, Lefeuvre E and Richard C 2005 *IEEE Trans. Ultrason. Ferroelectr. Freq. Control* **52** 584–95
[8] Lien I, Shu Y, Wu W, Shiu S and Lin H 2010 *Smart Mater. Struct.* **19** 125009
[9] Lefeuvre E, Badel A, Richard C and Guyomar D 2005 *J. Intell. Mater. Syst. Struct.* **16** 865–76
[10] Wu Y, Badel A, Formosa F, Liu W and Agbossou A E 2013 *J. Intell. Mater. Syst. Struct.* **24** 1445–58
[11] Lefeuvre E, Badel A, Brenes A, Seok S, Woytasik M and Yoo C 2017 *Smart Mater. Struct.* **26** 035065
[12] Lallart M, Wu W J, Hsieh Y and Yan L 2017 *Smart Mater. Struct.* **26** 115012
[13] Lallart M and Guyomar D 2008 *Smart Mater. Struct.* **17** 035030
[14] Liang J and Liao W H 2011 *IEEE Trans. Ind. Electron.* **59** 1950–60
[15] Long Z, Wang X, Li P, Wang B, Zhang X, Chung H S H and Yang Z 2021 *IEEE Trans. Power Electron.* **36** 9093–104
[16] Giusa F, Maiorca F, Noto A, Trigona C, Andò B and Baglio S 2014 *Sens. Actuators* A **212** 34–41
[17] Shih Y S, Vasic D and Wu W J 2016 *Smart Mater. Struct.* **25** 125013
[18] Chen Z, He J, Liu J and Xiong Y 2018 *IEEE Trans. Power Electron.* **34** 2427–40
[19] Liu W, Badel A, Formosa F, Zhu Q, Zhao C and Hu G D 2017 *IEEE Trans. Ind. Electron.* **65** 3899–909
[20] Liu H, Lee C, Kobayashi T, Tay C J and Quan C 2012 *Smart Mater. Struct.* **21** 035005
[21] Wu Y, Badel A, Formosa F, Liu W and Agbossou A 2014 *J. Intell. Mater. Syst. Struct.* **25** 1658–63
[22] Giusa F, Giuffrida A, Trigona C, Andò B, Bulsara A R and Baglio S 2013 *Sens. Actuators* A **198** 35–45
[23] Liu W, Formosa F, Badel A, Wu Y and Agbossou A 2014 *Sens. Actuators* A **216** 106–15
[24] Liu H, Liang J and Ge C 2015 *Appl. Phys. Lett.* **107** 141902
[25] Liu W, Qin G, Zhu Q and Hu G 2018 *Smart Mater. Struct.* **27** 117003
[26] Liang J and Liao W H 2011 *IEEE/ASME Trans. Mechatron.* **17** 1145–57